JOURNAL OF CARDIOVASCULAR MAGNETIC RESONANCE®
Vol. 6, No. 4, pp. 785–792, 2004

VELOCITY MAPPING

Retrospective Respiratory Motion Correction for Navigated Cine Velocity Mapping

Christof Baltes,[1] Sebastian Kozerke,[1] David Atkinson,[2] and Peter Boesiger[1,*]

[1]Institute for Biomedical Engineering, University and ETH Zurich, Zurich, Switzerland
[2]Division of Imaging Sciences, King's College, London, UK

ABSTRACT

In general, high spatial and temporal resolutions in cine cardiac imaging require long scan times, making breath-hold acquisition impossible in many cases. To enable free-breathing cardiac imaging, methods such as navigator gating were developed to reduce image artifacts due to respiratory motion. Nevertheless, residual image blurring is seen in images acquired late in the cardiac cycle. Image blurring itself hampers accurate blood flow quantification, especially in vessels exhibiting high flows during diastole. In the present work, the navigator gating and slice tracking method was extended by using navigator information to correct for in-slice motion components throughout the cardiac cycle. For this purpose, a standard two-dimensional (2D) cine phase contrast sequence with navigator gating and slice position correction was used, and navigator information was recorded along with the raw k-space data. In postprocessing, in-plane motion components arising from respiration during the actual data acquisition were estimated and corrected according to the Fourier shift theorem. In phantom experiments, the performance of the correction algorithm for different slice angulations with respect to the navigator orientation was validated. In vivo, coronary flow measurements were performed in 9 healthy volunteers. The correction algorithm led to considerably improved vessel sharpness throughout the cardiac cycle in all measured subjects [increase in vessel sharpness: 16 ± 11% (mean ± SD)]. Furthermore, these improvements resulted in increased volume flow rates [16 ± 13% (mean ± SD)] after retrospective correction indicating the impact of the method. It is concluded that retrospective respiratory motion corrections for navigated cine two-dimensional (2D) velocity mapping can correct for in-plane motion components, providing better image quality for phases acquired late in the cardiac cycle.

*Correspondence: Peter Boesiger, Ph.D., Institute for Biomedical Engineering, University and ETH Zurich, Gloriastrasse 35, Zurich CH-8092, Switzerland; Fax: ++41-1-632-1193; E-mail: boesiger@biomed.ee.ethz.ch.

DOI: 10.1081/JCMR-200036119
1097-6647 (Print); 1532-429X (Online)

Therefore, this method holds promise in particular for free-breathing coronary flow quantification.

Key Words: Respiratory motion correction; Cine imaging; Coronary flow quantification.

INTRODUCTION

Respiratory motion is one of the major challenges in free-breathing cardiac magnetic resonance (MR) imaging. If not compensated, it results in image degradation. Several techniques have been proposed to cope with respiratory motion (Huber et al., 2001; Jhooti et al., 2000; Wang et al., 1996; Weiger et al., 1997). Among the different methods, navigator echo based respiratory gating and slice tracking have gained most attention due to their simplicity (McConnell et al., 1997; Wang et al., 1996). These techniques have been shown to provide good motion compensation for short acquisition windows such as those used in coronary imaging (Stuber et al., 1999). It has been pointed out, that the temporal delay between the navigator echo acquisition and the actual image data collection has to be as short as possible to avoid image blurring (Spuentrup et al., 2002).

If cine data are acquired throughout the cardiac cycle, navigator-based gating and tracking proves efficient only for the first few cardiac phases after the navigator unless an additional navigator at the end of each cycle is incorporated (Nagel et al., 1999). Gating based on two navigators (one at the beginning and one at the end of each cardiac cycle) has the disadvantage of low gating efficiencies in the order of 20–30%. Accordingly, scan times are increased by a factor of up to five, reducing the feasibility of, for example, free-breathing coronary flow quantification.

An ideal setup for free-breathing cine imaging would incorporate multiple navigator echoes during the cardiac cycle, providing sufficient sampling of the respiratory curve. The actual slice position could then be prospectively corrected on a frame-by-frame basis using linear prediction theory (Nehrke et al., 1999). Such an implementation is, however, difficult due to the time necessary for acquiring and processing navigator echoes and the high temporal resolution required in coronary velocity mapping (Hofman et al., 1998).

Besides prospective respiratory motion compensation, a number of retrospective techniques have been proposed. Using an iterative approach, trial motions were applied to k-space to find a minimum in image entropy resulting in corrections for translational motion during image acquisition (Atkinson et al., 1997). Similar methods have also been used to retrospectively correct for uncertainties in the correlation factor between diaphragmatic and cardiac motion used in navigator based slice tracking (Atkinson et al., 2003; Wang and Ehman, 2000).

In this work, retrospective respiratory motion correction is introduced for navigated cine two-dimensional (2D) imaging of the heart. Using an additional navigator echo per cardiac cycle, considerable improvement of image quality for heart-phase images acquired later in the cardiac cycle can be achieved. To correct for variability of the correlation factor used to relate cardiac and diaphragmatic motion, the previously presented ''auto-focus'' technique (Atkinson et al., 2003) was integrated. For validation of the methods, phantom measurements were carried out. In vivo feasibility is demonstrated on data acquired with free-breathing coronary velocity mapping.

METHODS

Initial Considerations

Given that retrospective corrections can only be applied to correct for in-plane components of motion in 2D imaging, typical slice orientations and their relation to the main components of respiratory motion were investigated. Decompositions of the vector along the navigator direction into the components in measurement (M), phase-encode (P), and slice-select (S) directions were calculated. For typical angulations used in 2D cine coronary velocity mapping of the right coronary artery (RCA) (AP/FH/RL = 25°/4°/−10°), left anterior descending artery (LAD) (AP/FH/RL = 15°/−22°/0°), and coronary sinus (COS) (AP/FH/RL = −32°/−34°/−30°), the decomposition resulted in the following values (M/P/S): RCA: 0.90/0.14/0.42, LAD: 0.97/0.10/0.24, COS: 0.74/0.16/0.65. Small decomposition values in the slice-select (S) direction indicate only little residual motion through the imaging slice, which is important as retrospective corrections can only compensate for motion in-plane in the 2D imaging case. Accordingly, motion correction can be expected to work best for the LAD.

Phantom Validation

Phantom experiments were carried out to validate retrospective corrections for in-plane motion components in 2D imaging. Respiratory motion was simulated using a moving phantom. A water-filled bottle was fixed to the phantom probe head and was moved periodically with sinusoidal translational motion in feet-head (FH) direction. The peak-to-peak amplitude and frequency of the motion were adjusted to 30 mm and 10 cycles/min, respectively. A small tube (inner diameter: 5 mm) was attached to the bottle such that flow in the anterior-posterior (AP) direction could be simulated. An UHDC flow system (Shelley, London, Ontario, Canada) was used to generate steady flow rates at 4 ml/sec. The flowing water and the water inside the bottle were doped with 0.1 g/l $MnCl_2$, resulting in a T_1 of 270 ms. In addition, a water-filled syringe was attached to the phantom, allowing measurements of the actual phantom positions using navigator echoes.

In an initial pilot experiment, the slice tracking factor was varied (0.6, 0.8, 1.0) for a fixed gating window width of 5 mm to validate the algorithm used to determine the true correlation factor between motion detected by the navigator and motion in the image itself (Atkinson et al., 2003). Thereafter, velocity encoded data were obtained for a fixed tracking factor of 1.0 and a gating window width of 5 mm. The acquisition was repeated for different angulations (AP/FH/RL = 0.0°/0.0°/0.0° − 27.5°) of the 2D imaging slice with respect to the phantom motion to simulate settings used in vivo. Imaging parameters were: slice orientation: coronal, field of view (FOV): 136×230 mm^2, matrix: 154×256, encoding velocity (venc): 40 cm/s, echo time (TE): 4.5 ms, repetition time (TR): 9.5 ms, simulated heart rate: 63 beats/min.

Flow values of the measurements on the moving phantom were compared to reference values given by the flow system control unit.

In Vivo Measurements

In vivo experiments were performed in 9 healthy volunteers after informed consent had been obtained (7 males and 2 females). The coronary artery system was localized using established coronary MRA protocols (Stuber et al., 1999). Subsequently, a cross section of the left anterior descending artery (LAD) was planned on the MRA images and on corresponding maximum intensity projections (MIP). To find the optimal position for velocity mapping, this vessel cross section was imaged using a single breath-hold cine 2D balanced fast field echo (FFE) sequence. The acquired images were inspected to make sure that no artery bifurcation was contained in the slice over the cardiac cycle. The actual velocity mapping was performed with an in-plane resolution of 0.9×0.9 mm^2, while varying the rectangular FOV according to the volunteer's chest $(183-230) \times 230$ mm^2. High temporal resolutions were adjusted (36.0–37.7 ms) to reduce low pass filtering of the flow profiles (Hofman et al., 1998). Remaining imaging parameters were: TE: 4.3–4.6 ms, TR: 8.7–8.9 ms, venc: 30 cm/s. A 9-mm-thick slice was imaged with two signal averages to gain sufficient signal-to-noise ratio (SNR). Flow profiles in the LAD ($n=7$), left circumflex (LCX) ($n=1$) and RCA ($n=1$) were measured. Due to the lack of a noninvasive modality to reliably quantify blood flow in the coronary arteries, we obtained an additional data set in one healthy subject using gating on both leading and trailing navigators. These data served as reference. A validation of this method against intravascular ultrasound was reported by Nagel et al. (1999).

In all experiments, two navigator echoes were acquired in each cardiac cycle using the leading one for

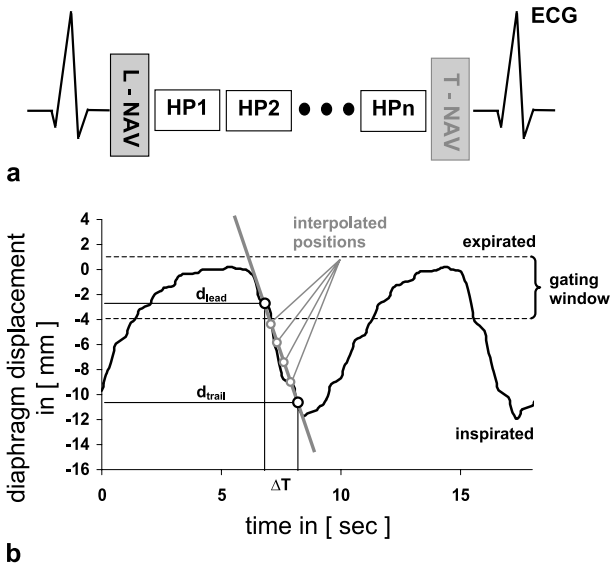

Figure 1. (a) Scheme of the ECG–triggered imaging sequence used to acquire multiple heart-phase images. Navigator gating and slice position correction was performed with the leading navigator (L-NAV). Data from both leading and trailing (T-NAV) navigators were recorded for retrospective image correction. (b) Exemplary respiratory curve (black solid) versus time to illustrate the interpolation approach described in Eq. 1. Linear interpolation (gray) between leading (d_{lead}) and trailing (d_{trail}) navigator was performed to estimate the diaphragm position (gray circle) for each heart phase.

gating and slice tracking (Fig. 1a). The trailing navigator was used for monitoring purposes. The acquired raw image data were saved into files along with the diaphragm positions measured by the navigators.

All experiments were performed on a commercial 1.5 T Intera MR system (Philips Medical Systems, Best, the Netherlands) equipped with a master gradient system (30 mT/m; 219 mT/m/ms). A circular surface coil (diameter: 20 cm) was used for the phantom experiments, while a dedicated five-element cardiac phased-array coil consisting of two circular anterior (diameter: 20 cm) and three rectangular posterior elements (14 cm $\times$ 20 cm) were used for the in vivo experiments.

Postprocessing

In postprocessing, k-space data were corrected using an algorithm written in IDL (Version 5.4, Research Systems Inc., Boulder, CO). The actual displacement (h_{FH}) of the region of interest in the heart was calculated according to the following equation:

$$h_{FH} = f_t \cdot \left(\frac{d_{trail} - d_{lead}}{\Delta T} \cdot t + d_{lead} \right) - f_c \cdot d_{lead} \quad (1)$$

The diaphragm displacement for each acquired profile was estimated by linear interpolation over time (t) between the leading (d_{lead}) and trailing (d_{trail}) navigator positions (Fig. 1b). Due to the coarse sampling of the respiratory positions, higher order interpolation schemes were not investigated. Subsequently, the diaphragm displacements were multiplied with a trial tracking factor (f_t) to account for possible inter-subject variability of the correlation between diaphragm and cardiac motion (Taylor et al., 1999). Corrections using a constant tracking factor (f_c) as applied by the regular scanner software were subtracted. The factor f_c was 1.0 in the phantom experiments and 0.6 (Wang et al., 1995) for all in vivo measurements. The resulting displacement (h_{FH}) was projected onto the imaging plane using scaling factors defined by the slice orientation with respect to the navigator orientation.

Rigid-body translational motion during the acquisition results in a linear phase in k-space according to the Fourier shift theorem. The additional phase (φ) at each k-space point in the measurement (M) and phase encoding (P) directions can be calculated by incorporating the scaling factors ($scale_{M,P}$) as follows:

$$\varphi_{M,P} = \frac{2\pi}{FOV_{M,P}} n \cdot scale_{M,P} \cdot h_{FH} \quad (2)$$

where $FOV_{M,P}$ denotes the field-of-view in the measurement and phase-encode directions and n the actual k-space matrix index. These linear phase terms were applied to k-space and then the images were reconstructed.

To account for variability of the slice tracking factor in vivo, different trial tracking factors were applied to find the optimal tracking factor. The algorithm was based on an objective image quality measure. In previous works, the entropy of the image gradients was found to be an optimal measure (Atkinson et al., 1997; McGee et al., 2000). In this study, the gradient image ($s_{i,j}$) was calculated by applying a Sobel filter (kernel size: 3 pixel) in both phase-encode and read-out direction and the corresponding entropy (E) was determined according to:

$$E = -\sum_{i,j} h_{i,j} \cdot \log_2(h_{i,j}) \quad where$$
$$h_{i,j} = \frac{s_{i,j}}{\sum_{i,j} s_{i,j}^2} \quad (3)$$

where i, j denote the image matrix indices. The entropy was calculated in a region of interest (ROI) and served as a measure for vessel sharpness.

A rectangular ROI containing the entire vessel and some surrounding tissue was manually drawn and copied to all heart phases. Subsequently, the center of the ROI was matched to the center of the vessel for each heart phase. To achieve one quality measure per

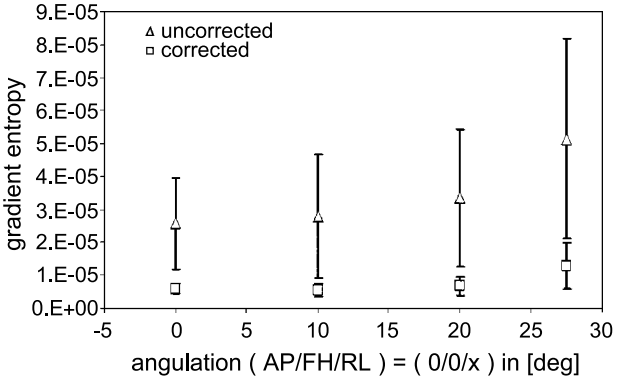

Figure 2. Phantom experiment. To investigate the performance of the correction algorithm, the image gradient entropy as measure for tube sharpness was determined for increasing slice angulations. Uncorrected data are indicated by triangles, corrected data by rectangles. Error bars represent standard deviations of image gradient entropy over the simulated cycle. The error bars of the corrected data were magnified by a factor of 10 for better visibility.

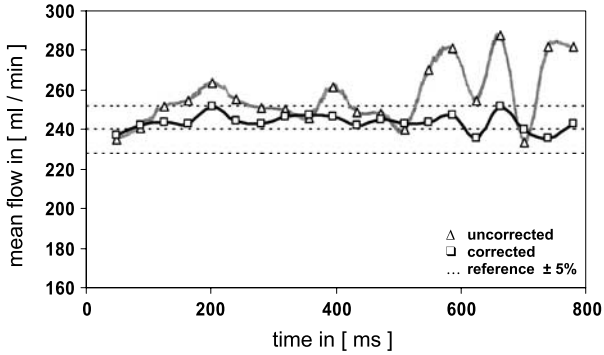

Figure 3. Phantom experiment. Mean flow values plotted over one simulated cycle for uncorrected (triangles) and corrected (rectangles) data. The dashed lines represent the reference flow value given by the flow system and its 5% limits.

trial tracking factor, the entropies over all cardiac phases were averaged. The optimal tracking factor was then found by varying the trial tracking factor from 0.2 to 1.0 in steps of 0.1. The trial factor yielding minimum entropy of the gradient image representing highest vessel sharpness was chosen to be the optimal tracking factor.

Data Evaluation

Flow calculation was performed before and after retrospective correction of the velocity maps. In the phantom data sets, a ROI was determined in the first cardiac phase of each measurement by taking the full width at 10% of the magnitude maximum (FWTM) (Hoogeveen et al., 1998). This ROI was then copied to all heart phases and the center of each ROI was shifted to match the center of the tube. Subsequently, the mean flow and its standard deviation were calculated over one cardiac cycle.

In the in vivo data sets, the ROIs representing the vessel of interest were manually drawn for each heart phase. Additional ROIs were placed on the adjacent myocardium to quantify cardiac through-plane motion over the cardiac cycle. The velocity of this additional motion was subtracted from the blood velocity data inside the coronary artery. Subsequently, mean flow for each heart phase and volume flow was calculated.

RESULTS

Phantom Validation

In postprocessing, the correct tracking factor of 1.0 was determined for all phantom experiments including all experiments in which the tracking factor was varied.

Figure 2 shows the image gradient entropy for different angulations of the imaging slice with respect to the navigator direction. The gradient entropy metric is plotted versus slice angulation before (rectangles) and after (triangles) correction with error bars indicating the standard deviation of the gradient entropy over the cardiac cycle. For all angulations a significant improvement in vessel sharpness was achieved by the correction algorithm. Not only did the mean values of the metric decrease, but also the standard deviations were reduced (Fig. 2: error bars of corrected data are

Table 1. Diaphragm displacements, slice angulations and optimal tracking factors for in vivo measurements.

				Slice Ang. (deg)			Projection			
Vol.	Loc.	Displ. (mm)	Eff. (%)	AP	FH	RL	M	P	S	Opt. TF
1	LAD	3.82±3.25	53	18.0	−17.4	0.0	0.95	0.09	0.30	0.6
2	LAD	5.13±4.05	42	26.5	−26.7	0.2	0.90	0.20	0.40	0.7
3	LAD	4.45±3.91	54	19.8	−31.5	0.0	0.94	0.18	0.29	0.2
4	LCX	3.62±1.93	39	11.4	32.7	0.0	0.98	0.11	0.17	0.5
5	LAD	3.49±4.52	55	11.0	−14.3	0.0	0.98	0.05	0.19	0.4
6	LAD	5.23±3.58	53	2.3	−19.4	0.0	0.99	0.01	0.04	0.4
7	LAD	1.33±3.21	73	16.5	−26.0	0.0	0.96	0.13	0.26	0.8
8	LAD	7.86±4.07	33	10.1	−18.0	0.0	0.98	0.05	0.17	0.2
(8 ref	LAD	1.92±1.15	17	10.1	−18.0	0.0	0.98	0.05	0.17	0.3)
9	RCA	3.80±3.31	47	27.5	5.4	−11.5	0.47	−0.16	0.87	0.9

Abbreviations: Vol.=volunteer; Loc.=location; Displ.=diaphragm displacement given as mean ± SD; Eff.=gating efficiency; Slice Ang.=slice angulation; Projection=projection of feet-head motion onto imaging slice components (M=measurement direction; P=phase-encode direction; S=slice-select direction); Opt. TF=optimal tracking factor.

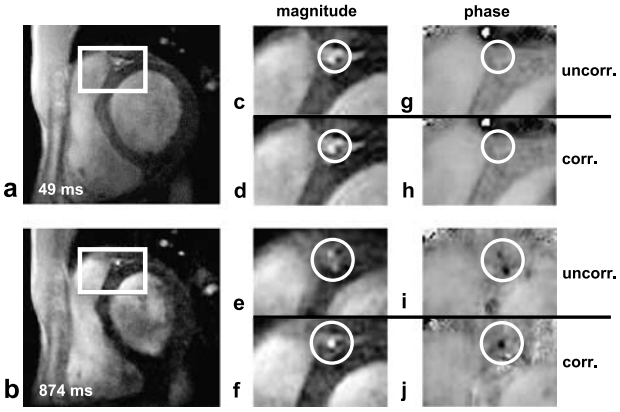

Figure 4. In vivo experiment. Anatomical images and velocity maps acquired 49 ms and 874 ms after the ECG trigger in one representative volunteer. An overview of the heart is shown in (a) and (b), where the area of the LAD is indicated by white rectangles. In the first heart phase, image quality is comparable for both the uncorrected (c, g) and the corrected (d, h) data. In contrast, considerable improvement in image quality and vessel sharpness of the LAD (circles) is seen in the later heart phase (f, j, compared to e, i).

multiplied by a factor of 10). According to theory, the efficiency of the correction reduces for increasing slice angulations (AP/FH/RL = 0.0°/0.0°/27.5°) (Fig. 2). Phantom experiments revealed that motion correction works for through-plane motion components up to 0.46 (RL = 27.5°).

Figure 3 shows flow values extracted from uncorrected and corrected data over the simulated cycle. Considerable deviation of the uncorrected flow values from the reference values is seen for later phases. After corrections, the accuracy of flow quantification increased significantly, so that all flow values lie within the 5% limits of the reference values.

In Vivo Measurements

In Table 1, subject dependent parameters of the in vivo acquisitions are listed. The diaphragm displacement between leading and trailing navigator for all accepted cardiac cycles is given as mean ± standard deviation (SD), indicating the extent of respiratory motion during the acquisition ranging from 1.33 ± 3.21 mm to 7.86 ± 4.07 mm. In addition, the efficiency of the correction algorithm can be estimated by the listed slice angulation and the corresponding scaling factors.

Figure 4 depicts representative anatomical images (magnitude) and velocity maps (phase) acquired at the beginning (49 ms) and at the end (874 ms) of the cardiac cycle (volunteer #2). In the overview of the heart (Figs. 4a and 4b) the area of the LAD is marked by white rectangles. The impact of corrections on the sharpness of the LAD (circles) is emphasized by comparing the images before (Figs. 4c, 4g, 4e, and 4i) and after (Figs. 4d, 4h, 4f, and 4j) corrections. Image quality and vessel sharpness were not affected to a large extend by retrospective corrections of the first heart phases following the navigator. The temporal proximity to the leading navigator resulted in comparable image quality for both the uncorrected (Figs. 4c and 4g) and the corrected (Figs. 4d and 4h) data. In contrast, image quality improved significantly with retrospective corrections of later heart phases, e.g., 874 ms after the ECG trigger. In this case, corrections not

Table 2. Vessel sharpness represented by the entropy of the gradient images and volume flow rates of the in vivo measurements.

			Vol. flow (ml/min)			
Vol.	Loc.	Increase of VS (%)	Uncorr.	Corr.	Change (%)	Heart rate (beats/min)
1	LAD	27	748	1071	43	79
2	LAD	31	1159	1381	19	48
3	LAD	4	705	735	4	61
4	LCX	21	803	931	16	68
5	LAD	5	974	1170	20	48
6	LAD	18	1267	1321	4	53
7	LAD	1	717	705	−2	65
8	LAD	12	1095	1284	17	59
(8 ref	LAD	–	–	1198	–	59)
9	RCA	23	1001	1180	18	57
		16 ± 11			16 ± 13	

Abbreviations: Vol. = volunteer; Loc. = location; Increase of VS = increase of vessel sharpness compared to uncorrected data; Vol. Flow = volume flow rate.

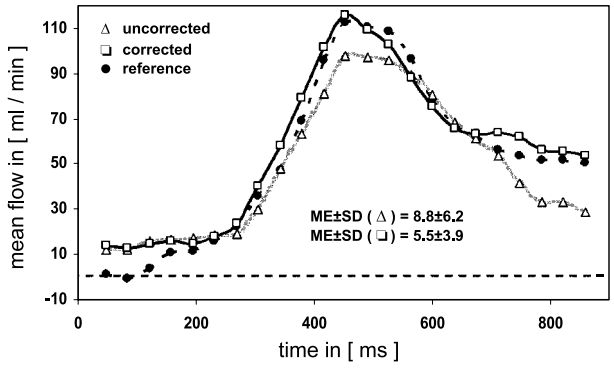

Figure 5. In vivo experiment. Flow profiles versus time obtained in volunteer #8. The uncorrected (triangles) and corrected (rectangles) profiles differ significantly during systole and mid-diastole, resulting in varying volume flow rates (Table 2). The flow profile obtained after retrospective corrections approximates the reference profile (circles) more closely, as indicated by the mean error (ME). The reference profile was obtained with gating on both leading and trailing navigators.

only improved image quality and vessel sharpness, but also removed ghosting artifacts (two vessels, Figs. 4e and 4i) resulting in one distinct vessel (Figs. 4f and 4j). Motion corrections resulted in reduced gradient entropy values compared to the uncorrected data, as listed in Table 2. According to theory, the decrease in entropy of the gradient images is associated with an increase in vessel sharpness.

Besides improved vessel sharpness, flow profiles in the vessels over the cardiac cycle were also altered, as shown in Fig. 5 for image data before (triangles) and after (rectangles) corrections. Since the actual flow profile was unknown, a reference profile (circle) was acquired with gating on both leading and trailing navigator. Accordingly, only the tracking factor was corrected in postprocessing. As indicated by the mean error (ME), the reference profile is more closely approximated by the corrected data (Fig. 5). In Table 2, volume flow rates for all volunteers are listed before and after correction. On average, volume flow rates increased by $16 \pm 13\%$ (mean ± SD) after retrospective corrections.

DISCUSSION

In the present work, phantom experiments and in vivo measurements on healthy volunteers were carried out to investigate retrospective corrections for respiratory motion during navigated 2D cine MR velocity mapping.

In phantom experiments, the performance of the algorithm was validated for deliberately altered tracking factors. In all experiments the correct tracking factor was found.

The efficiency of the correction algorithm depends on the extent of the through-plane motion component indicated by the scale factor in the slice-select direction. Thus, the approach might be less efficient for slice orientations used in velocity mapping of the right coronary artery and the coronary sinus.

The accuracy of flow quantification improved consistently after retrospective corrections, as shown in the phantom experiments.

In vivo feasibility of the correction algorithm was demonstrated in 9 healthy volunteers (7 male and 2 female). Using retrospective corrections, improved image quality and vessel sharpness were obtained throughout the cardiac cycle.

Although the retrospective correction resulted in slightly different optimal tracking factors for the reference measurement [Vol. 8 (ref)] and the standard sequence (Vol. 8), as depicted in Table 1, a good agreement of the flow profiles and the volume flow rates was obtained after the correction. This difference in the optimal tracking factor might be related to round-off errors associated with the step size of 0.1 used for the trial tracking factors.

Although a reduced efficiency of the retrospective correction for data acquired in the RCA was predicted, in vivo results showed nevertheless considerable improvement in vessel sharpness in one exemplary dataset (Table 2). This illustrates that motion correction can even be used to correct images acquired in the RCA though the impact of correction might vary taking into account a larger number of study subjects.

The acquisition of trailing navigators is not essential (Fig. 1a). Due to the short temporal delay between the trailing navigator and the leading navigator of the next cardiac cycle, little additional information on the respiratory motion is gained. As a consequence, the trailing navigator could be omitted, which would enable data acquisition for an additional cardiac phase instead. In this case, diaphragm positions throughout the cardiac cycle would be estimated based on interpolation between two successive leading navigators.

In conclusion, a retrospective approach to correct for respiratory in-plane motion of 2D cine velocity maps was presented. Efficiency and accuracy of the approach were validated in phantom experiments. The algorithm proved to be particularly efficient in correcting image artifacts in heart-phase images acquired later in the cardiac cycle. Improved image quality and vessel sharpness resulted in more accurate velocity

quantification, indicating the potential of the method for free-breathing, cine velocity mapping.

ACKNOWLEDGMENTS

The authors would like to thank Steffen Ringgaard and Ernst-Torben Fruend from the University Hospital Aarhus, Denmark, for lending the UHDC flow system and for their technical support. Furthermore, the authors are grateful to Philips Medical Systems (PMS) for technical and financial support. This work is in part funded by the ETH Zurich (SEP). D. A. thanks the UK EPSRC for funding (grant ARF/001381).

REFERENCES

Atkinson, D., Hill, D. L., Stoyle, P. N., Summers, P. E., Keevil, S. F. (1997). Automatic correction of motion artifacts in magnetic resonance images using an entropy focus criterion. *IEEE Trans. Med. Imag.* 16:903–910.

Atkinson, D., Kozerke, S., Razavi, R. (2003). Retrospective image correction combined with slice tracking for respiratory motion compensation. *J. Cardiovasc. Magn. Reson.* 5:270–271.

Hofman, M. B., Wickline, S. A., Lorenz, C. H. (1998). Quantification of in-plane motion of the coronary arteries during the cardiac cycle: implications for acquisition window duration for MR flow quantification. *J. Magn. Reson. Imaging* 8:568–576.

Hoogeveen, R. M., Bakker, C. J., Viergever, M. A. (1998). Limits to the accuracy of vessel diameter measurement in MR angiography. *J. Magn. Reson. Imaging* 8:1228–1235.

Huber, M. E., Hengesbach, D., Botnar, R. M., Kissinger, K. V., Boesiger, P., Manning, W. J., Stuber, M. (2001). Motion artifact reduction and vessel enhancement for free-breathing navigator-gated coronary MRA using 3D k-space reordering. *Magn. Reson. Med.* 45:645–652.

Jhooti, P., Gatehouse, P. D., Keegan, J., Bunce, N. H., Taylor, A. M., Firmin, D. N. (2000). Phase ordering with automatic window selection (PAWS): a novel motion-resistant technique for 3D coronary imaging. *Magn. Reson. Med.* 43: 470–480.

McConnell, M. V., Khasgiwala, V. C., Savord, B. J., Chen, M. H., Chuang, M. L., Edelman, R. R., Manning, W. J. (1997). Comparison of respiratory suppression methods and navigator locations for MR coronary angiography. *AJR Am. J. Roentgenol.* 168:1369–1375.

McGee, K. P., Manduca, A., Felmlee, J. P., Riederer, S. J., Ehman, R. L. (2000). Image metric-based correction (autocorrection) of motion effects: analysis of image metrics. *J. Magn. Reson. Imaging* 11:174–181.

Nagel, E., Bornstedt, A., Hug, J., Schnackenburg, B., Wellnhofer, E., Fleck, E. (1999). Noninvasive determination of coronary blood flow velocity with magnetic resonance imaging: comparison of breath-hold and navigator techniques with intravascular ultrasound. *Magn. Reson. Med.* 41:544–549.

Nehrke, K., Boernert, P., Boeck, J. C. (1999). Prediction and interpolation of motion states for real-time respiratory gating. *Proc. 16th Annual Meeting ESMRMB*. 167–168.

Spuentrup, E., Manning, W. J., Botnar, R. M., Kissinger, K. V., Stuber, M. (2002). Impact of navigator timing on free-breathing submillimeter 3D coronary magnetic resonance angiography. *Magn. Reson. Med.* 47:196–201.

Stuber, M., Botnar, R. M., Danias, P. G., Sodickson, D. K., Kissinger, K. V., Van Cauteren, M., De Becker, J., Manning, W. J. (1999). Double-oblique free-breathing high resolution three-dimensional coronary magnetic resonance angiography. *J. Am. Coll. Cardiol.* 34:524–531.

Taylor, A. M., Keegan, J., Jhooti, P., Firmin, D. N., Pennell, D. J. (1999). Calculation of a subject-specific adaptive motion-correction factor for improved real-time navigator echo-gated magnetic resonance coronary angiography. *J. Cardiovasc. Magn. Reson.* 1:131–138.

Wang, Y., Ehman, R. L. (2000). Retrospective adaptive motion correction for navigator-gated 3D coronary MR angiography. *J. Magn. Reson. Imaging* 11:208–214.

Wang, Y., Riederer, S. J., Ehman, R. L. (1995). Respiratory motion of the heart: kinematics and the implications for the spatial resolution in coronary imaging. *Magn. Reson. Med.* 33:713–719.

Wang, Y., Rossman, P. J., Grimm, R. C., Riederer, S. J., Ehman, R. L. (1996). Navigator-echo-based real-time respiratory gating and triggering for reduction of respiration effects in three-dimensional coronary MR angiography. *Radiology* 198:55–60.

Weiger, M., Bornert, P., Proksa, R., Schaffter, T., Haase, A. (1997). Motion-adapted gating based on k-space weighting for reduction of respiratory motion artifacts. *Magn. Reson. Med.* 38:322–333.

Submitted September 25, 2003
Accepted April 7, 2004